Patric Berger, Clemens Schmetterer, Herta Silvia Effenberger and Hans Flandorfer*

The ternary phase $Li_8Sb_xSn_{3-x}$ with $0.3 \leq x \leq 1.0$

https://doi.org/10.1515/zkri-2020-0020
Received February 26, 2020; accepted April 22, 2020;
published online June 3, 2020

Abstract: In the frame of the studies on the phase relations in the ternary system Li–Sb–Sn at 300 °C the new ternary phase $Li_8Sb_xSn_{3-x}$ ($0.3 \leq x \leq 1.0$) was synthesized and characterized predominantly by single crystal and powder X-ray diffraction. The title compound crystallizes trigonally in the space group $R\bar{3}m$ (no. 166), the lattice parameters are a = 4.6962(11) Å and c = 31.536(6) Å. The crystal structure of $Li_8Sb_xSn_{3-x}$ is described in the present paper. In addition, the stereochemical and topological relations to the phases with similar composition, namely $Li_{13}Sn_5$, Li_5Sn_2 as well as cubic Li_3Sb, besides native Li are discussed.

Keywords: crystal structure; hexacapped cube; Li–Sb–Sn; $Li_8Sb_xSn_{3-x}$; X-ray diffraction.

1 Introduction

Currently employed rechargeable Li-ion batteries (LiBs) are widely applied in handheld electronics such as notebooks, cell phones or cameras. However, for high-power applications, like stationary storage systems or electric mobility, they are insufficient in terms of capacity and cyclability. To improve the performance of today's LiBs, further developments are required for the three fundamental constituents, namely the anode, the cathode and the electrolyte.

For the anode, intermetallic materials seem possible alternatives to the commonly used graphite (372 mAh g^{-1}), since e. g. Sb and Sn show theoretical specific capacities of 660 and 994 mAh g^{-1}, respectively [1]. Unfortunately, expected volume changes during (de)lithiation lead to mechanical degradation of the electrode and restrict the lifetime of respective batteries. One tentative possibility to overcome this limitation is the use of Sb–Sn alloys instead of the pure elements only [2–4]. Lithiation of these alloys starts with the formation of the phase Li_3Sb going along with the precipitation of Sn. The fine grained tin matrix can buffer mechanical stress from formation of lithiated phases. Another possibility to overcome these drawbacks is the co-precipitation of a material which is completely inactive against lithium (like the transition metals Ti or Nb), in combination with the formation of lithiated Sb- and Sn-compounds. Especially the ternary compounds SbSnTi and $Ti_{1-y}Nb_ySnSb$ ($0 \leq y \leq 1$) have been studied in detail [5, 6]. The lithiation path of these ternary compounds, synthesized by ball milling of the pure elements, was investigated by operando-X-ray diffraction (XRD) and Mössbauer techniques and resulted in a simultaneous conversion to Li–Sb and Li–Sn alloys during the lithiation process in which pure transition metals are precipitated contemporaneously. Thereby, Li_3Sb and Li_7Sn_2 represent the highest lithiated phases. However, the authors have not been aware of phase relations in Li–Sb–Sn and Ti–Sb–Sn. In order to understand, control and design the (de)lithiation processes, further and detailed knowledge about relevant phases, phase transitions, thermodynamic properties and crystal structures of the involved phases is indispensable.

The Li–Sn system [7] contains at least seven intermetallic compounds which exhibit narrow homogeneity ranges. Five of them are Li-rich and close in composition where the $Li_{17}Sn_4$ compound is the richest in Li. In addition to the seven well described intermetallic phases, there are hints from e.m.f. investigations for a further compound, Li_8Sn_3 [8, 9]. Interestingly, in the Li–Pb system, an equilibrium compound Li_8Pb_3 was found [10, 11], while in the Li–Sn system the existence of the corresponding analogue was never proved or described by means of thermal analysis or crystal structure investigations. So far, this compound has not yet been isolated or structurally characterized; calculations of the stability or the electronic properties are available from [12], who calculated the formation energy of several thousands of hypothetical Li–Sn compounds using various crystal structures through discrete Fourier transform (DFT). From these they selected those with the lowest formation energies as possibly stable phases in addition to the known ones, including Li_8Sn_3. However,

***Corresponding author: Hans Flandorfer**, Institute of Inorganic Chemistry - functional Materials, University of Vienna, Faculty of Chemistry, Althanstraße 14 (UZAII), 1090 Vienna, Austria,
E-mail: hans.flandorfer@univie.ac.at
Patric Berger: Institute of Inorganic Chemistry – functional Materials, University of Vienna, Faculty of Chemistry, Althanstraße 14 (UZAII), 1090 Vienna, Austria
Clemens Schmetterer: Institute of Physical Chemistry, University of Vienna, Faculty of Chemistry, Waehringerstraße 42, 1090 Vienna, Austria
Herta Silvia Effenberger: Institute of Mineralogy and Crystallography, University of Vienna, Faculty of Geosciences, Geography and Astronomy, Althanstraße 14 (UZAII), 1090 Vienna, Austria

none of these additional compounds have been found so far and described through experiments. Furthermore, their calculations are only valid for a temperature of 0 K.

In the Li–Sb system [13], the most Li-rich compound is Li_3Sb [14, 15], the second stable phase is Li_2Sb. Phase diagrams of both systems exhibit similarities in their general outline (steep Li-rich liquidus line and high melting regime), but differ in the type and number of intermetallic phases. The system Sb–Sn was recently discussed and described in detail by Schmetterer et al. [16, 17]. The well-known Sb–Sn phase which exhibits a large homogeneity range was found to be incommensurately modulated, the compound Sb_2Sn_3 was proved to be an artifact while a new commensurate phase Sb_3Sn_4 with small homogeneity range was established.

There is no clear evidence for a ternary compound in Li–Sb–Sn from literature. Rönnebro et al. [18] report a compound $Li_{2.78}Sn_{0.22}Sb$ which was supposed to form by the lithiation of an Ag–Sb–Sn alloy ($Ag_{36.4}Sb_{15.6}Sn_{48}$) by ball milling. The existence of such a phase was discussed in more detail in another paper [19] by the same group doing electrochemical lithiation of $Ag_{36.4}Sb_{15.6}Sn_{48}$. However, the evaluation of powder-XRD (PXRD) patterns is not at all convincing. Positions and intensities of peaks allocated to $Li_{2+x}SbSn_{1-x}$ cannot be distinguished from these of Li_3Sb which is as well formed on lithiation. In addition, a further isotypic phase, $Ag_{2-x}Li_{1+x}Sn$ is present in some of the alloys investigated, whose XRD-pattern can hardly be distinguished from a hypothetic $Li_{2+x}SbSn_{1-x}$. No single crystals were measured and for our opinion there is no clear proof for the existence of such a Li–Sb–Sn compound.

During our work on the phase diagram of the ternary Li–Sb–Sn system, the existence of a new ternary Li-rich compound was indicated from powder X-ray patterns of several samples showing additional but comparable diffraction peaks. From the single-crystal structure refinement the chemical formula $Li_8Sb_xSn_{3-x}$ ($0.3 \leq x \leq 1.0$) was derived.

2 Experimental

2.1 Synthesis

For sample preparation, pure Li wire (Alfa Aesar, 3.2 mm, 99.8%, with oil coating) which was stored in a glovebox under Ar atmosphere (Ar 5.0; $O_2 < 1$ ppm; $H_2O < 1$ ppm), tin rods (Alfa Aesar, 999985) and Sb (Alfa Aesar, ingot, 99,999%) were used. Initially, the lithium wire was cleaned outside the glovebox in an ultrasonic bath in cyclohexane, followed by vacuum evaporation of the solvent in the antechamber of the glovebox. Surface oxidation products of the lithium wire caused by short time exposure to air were mechanically scraped off with a shear before use. Sb was further purified by filtration of the liquid metal through quartz glass wool under vacuum.

The single crystal for the present structure determination was selected from a sample with input composition $Li_{75}Sb_{12.5}Sn_{12.5}$ that was initially prepared for the determination of the phase equilibria. This sample was made through weighing the required amounts of the pure elements inside a glovebox (Ar 5.0; $O_2 < 1$ ppm; $H_2O < 1$ ppm) and put into a tantalum crucible. The Ta-crucible was placed on a water cooled Cu mount in an electric arc furnace and sealed by arc welding under Ar-atmosphere after evacuating and flushing the chamber of the arc furnace three times. The sealed crucible was transferred into an induction furnace, where the sample was melted at 1,000 °C for 10–20 s. To ensure homogeneous mixing of the elements, the melting process was repeated twice with turning the Ta-crucible upside down after each melting sequence. In a final step, the crucible itself was sealed in a quartz glass tube under vacuum and annealed at 300 °C in a muffle furnace for four weeks. Thereafter, the sample was quenched in cold water, put back to the glovebox again and opened with a crusher. The PXRD pattern of the above mentioned sample $Li_{75}Sb_{15}Sn_{15}$ shows the ternary phase $Li_8Sb_xSn_{3-x}$ besides the binary Li_3Sb (Figure 1), which is in accordance with preliminary phase diagram data from work in progress. The broad humps in the background stem from the amorphous polycarbonate cap of the sample holder (see below).

2.2 Powder X-ray diffraction (PXRD)

Small amounts of the obtained alloy were powdered in a glovebox using a Durit® mortar. Powder patterns were recorded on a Bruker D8 diffractometer with Bragg-Brentano pseudo-focusing geometry (θ/2θ-geometry) with $Cu_{K\alpha}$ X-radiation (40 kV/40 mA/Ni filter). The scattered intensities were detected using a one dimensional Si-strip detector (LynxEye detector, Bruker, Germany). The powdered alloy was fixed with dried petroleum jelly on a silicon-single crystal, which served as sample holder. To prevent oxidation of the powder during the measurement, the sample was covered by a polycarbonate cap with an O-ring tightening under Ar-atmosphere. For phase analysis full profile Rietveld-refinement was applied using Topas4® software supplied by Bruker, Germany.

2.3 Single-crystal X-ray diffraction (SCXRD)

A small crystal chip of the title compound was fixed with and covered by vacuum grease on a glass capillary. Multiple trials were necessary to find a single crystal of sufficient quality for X-ray data collection. For investigations, a four-circle Nonius Kappa diffractometer was used (charge-coupled device (CCD) detector, 300 μm capillary optics collimator, conventional X-ray tube, monochromated $Mo_{K\alpha}$ radiation). To prevent decomposition of the samples in air, the crystals were kept in a dry N_2-gas stream at 290 K during the measurement. The unit-cell parameters were obtained by least-squares refinements from the 2ϑ values of the positions of the measured Bragg reflections. Corrections for Lorentz polarization and absorption effects (multi-scan method) were applied; complex scattering functions [20] were used. For data collection, structure solution and refinements served the programs “Collect” [21, 22], “SHELXS-97” and “SHELXL-97” [23–26]. Reflection statistics

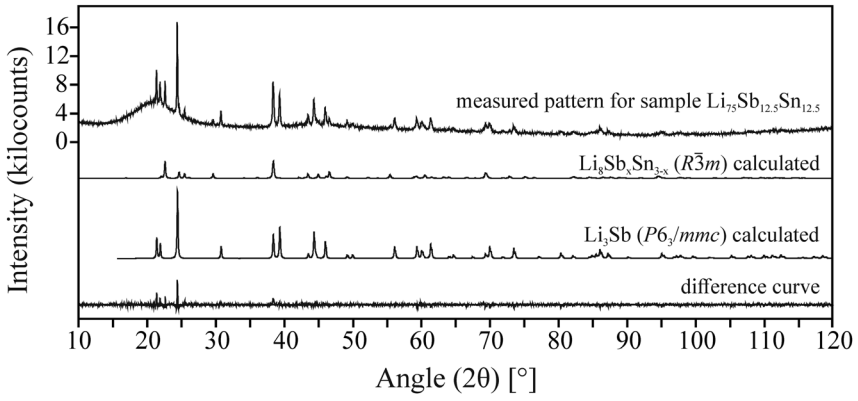

Figure 1: Powder X-ray diffraction (PXRD) pattern of the sample obtained from an input $Li_{75}Sb_{12.5}Sn_{12.5}$: observed, calculated and difference pattern.

suggested *centro*symmetry. The extinction symbol and possible space-group symmetries were found from the extinction rules; $R\bar{3}m$ is evident from structure refinements. The two positions of the atoms *M* = (Sb and/or Sn) were obtained by direct methods in combination with Patterson summations. Successive Fourier and difference Fourier summations revealed the four remaining atom sites.

3 Results and discussion

3.1 Crystal structure determination and refinements

In the first step of the structure refinement the scattering functions of Sb and Li were applied for the two *M* (=Sn, Sb) and four Li sites. However, for the Li1 site a slight excess in the electron density was observed due to a minor substitution by *M* atoms. During the refinement full occupation was assumed for the Li1 site but the ratio of scattering function Sn:Li was allowed to vary. However, one cannot exclude a larger amount of *M* atoms going along with the formation of vacancies.

As the chemical elements Sb and Sn are adjacent in the periodic table, a distinction using conventional X-ray sources is not likely although there is a hint for the distribution of Sb and Sn on the *M*1 and *M*2 position, respectively. The R values change slightly for structure models based on distinct scattering functions used. Trials using the scattering functions Sb/Sb – Sb/Sn – Sn/Sb – Sn/Sn for the atomic positions *M*1/*M*2, respectively, result in the following residual values R1(all reflections)/R1(observed reflections)/wR2: 0.026/0.020/0.043 – 0.024/0.019/0.044 – 0.029/0.024/0.046 – 0.026/0.021/0.046. The refinements of these distinct structure models give a hint that Sb atoms may show a site preference for the *M*1 position 3(*a*), and Sn atoms for the *M*2 6(*c*) position. It is consistent with the expected Sb:Sn ratio of 1:2 and result ideally in an ordered atomic arrangement with respect to the two *M* positions. Such a preferred occupation is supported by crystal chemical considerations (see Section 3 below).

Somewhat large isotropic displacement parameters were obtained for the positions Li2 and Li3. It should be mentioned that the r.m.s. amplitudes of these two atom sites indicate an approximate isometric behavior: 0.034 and 0.031 Å^2 parallel to [001] respectively and 0.027 and 0.030 Å^2 in (00.1). The displacement parameters of the Li2 and Li3 atoms indicate a somewhat too high scattering power assumed in the actual structure model; minor vacancies at these two sites are feasible. Due to high correlation terms with the displacement parameters the refinement of the two site occupation factors is not significant. A partial substitution at all the Li position by *M* atoms going along with the formation of a significant amount of vacancies cannot be ruled out. The calculated volume of the coordination polyhedra around the four crystallographically different Li atoms compare well (see Table 2).

Details of data collection and structure refinements are compiled in Table 1, structural parameters and interatomic distance in Table 2 (including [27–29]) and 3, respectively. The display of the crystal structures is based on the software ATOMS.

3.2 A note on the composition of the title compound

Prior to the description of the crystal structure, it is necessary to address the topic of the composition of the compound that arises from the presence of Li and the distribution of Sb and Sn.

It is impossible to determine the accurate composition of Li-containing materials by scanning electron microscope (SEM)/energy dispersive X-ray analysis (EDX)

analysis since the intensity of the X-ray emission of Li is too low. Calculations of the Li-content from residual mass are highly inaccurate because of the low atomic mass of Li, especially compared to this of Sb/Sn. In addition, preparation of samples for SEM/EDX is seriously complicated by the reaction of Li-alloys with air and moisture as well as the decomposition in the vacuum chamber during the electron irradiation. Further analytical methods are not applicable as the synthesized samples are not phase pure. Individual aggregates are small and intergrowth of distinct phases always is observed. Moreover, the individual phases cannot be identified in the optical microscope as the appearance is practically identical. Consequently, the separation of a sufficient amount of phase pure material of the compound under investigation was not possible. The stoichiometric formulation of this new ternary structure in respect to the Sb/Sn ratio is therefore given as $Li_8Sb_xSn_{3-x}$. Preliminary phase diagram data suggest a lower limit of ~3–4 at.% Sb; see also the last paragraph of this chapter. As discussed above, the structure model with Sb and Sn atoms occupying (predominantly) the *M*1 and *M*2 sites resulted in

Table 1: Single-crystal X-ray data-collection and structure refinements of $Li_8Sb_xSn_{3-x}$. Cell parameter obtained from PXRD are given in brackets.

a [Å]	4.6962(11) [4.6975(2)]
c [Å]	31.536(6) [31.538(2)]
Space group	$R\bar{3}m$ (no. 166)
V [Å^3]	602.3
Z	3 {$Li_{7.94}Sn_{2.06}Sb$}
ρ_{calc} [g cm^{-3}]/μ(Mo*Kα*) [mm^{-1}]	3.49/9.6
Crystal dimensions [μm]	70 × 80 × 90
Range of data collection ($\pm h \pm k \pm l$) [°]	$3 < 2\vartheta < 70$
Number of images/rotation angle per image [°]	1294/2
Scan mode (at 11 distinct ω-angles)	ϕ-scans
Scan time [s/°]/frame size (binned mode)	65/621 × 576 pixels
Detector-to-sample distance [mm]	32
Measured reflections	2205
Unique reflections (*n*)/reflections with $F_o > 4\sigma(F_o)$	388/352
$R_{int} = \Sigma\lvert F_o^2\text{-}F_o^2(\text{mean})\rvert/\Sigma F_o^2$	0.039
Extinction parameter *k*: $F_c^* = F_c \cdot k[1 + 0.001 \cdot F_c^2\lambda^3/\sin(2\vartheta)]^{-1/4}$	0.0019(3)
$R1 = \Sigma(\lvert\lvert F_o\rvert - \lvert F_c\rvert\rvert)/\Sigma F_o$ (for 388/352 reflections)	0.024/0.019
$wR2 = [\Sigma w(F_o^2-F_c^2)^2/\Sigma\lvert wF_o^4\rvert]^{1/2}$	0.044
GooF = $\{\Sigma[w(F_o^2-F_c^2)^2]/(n-p)\}^{0.5}$	1.06
Max Δ/σ; number of variable parameters (*p*)	< 0.001; 20
Final difference Fourier map [eÅ^{-3}]	−0.79 to +0.86
$w = 1/\{\sigma^2(F_o^2) + [0.024 \times P]^2 + 0.75 \times P\}$; $P = ([\max(0,F_o^2)] + 2 \times F_c^2)/3]$	

Table 2: Fractional atomic coordinates and displacement parameters of $Li_8Sb_xSn_{3-x}$.

Atom	Scattering function	Wyckoff letter	Site symmetry	*z*	U_{equiv}	U_{11}	U_{33}	U_{12}	V [Å^3]	CN (H)	CN (O'K)
*M*1	$Sb_{1.0}$	3(*a*)	$\bar{3}m$	0	0.01668(13)	0.0171(2)	0.01582(2)	0.00856(7)	18.0	9.9	9.6
*M*2	$Sn_{1.0}$	6(*c*)	3*m*	0.454744(8)	0.01728(14)	0.0183(2)	0.0153(2)	0.00914(7)	18.5	10.4	10.3
Li1	$Li_{0.964}Sn_{0.036(2)}$	6(*c*)	3*m*	0.08913(12)	0.0159(13)	0.018(2)	0.013(2)	0.0087(8)	18.2	9.6	9.3
Li2	$Li_{1.0}$	6(*c*)	3*m*	0.1776(3)	0.030(2)	0.027(3)	0.034(4)	0.0137(14)	18.2	9.6	9.3
Li3	$Li_{1.0}$	6(*c*)	3*m*	0.2731(2)	0.031(2)	0.030(3)	0.031(5)	0.015(2)	18.4	10.0	9.9
Li4	$Li_{1.0}$	6(*c*)	3*m*	0.3631(2)	0.0148(14)	0.013(2)	0.019(3)	0.0064(9)	18.1	10.1	9.9

The anisotropic displacement parameters are defined as: $\exp[-2\pi^2\Sigma_i^3 = 1\,\Sigma_j^3 = 1\,U_{ij}a^*_i a^*_j h_i h_j]$. $x = y = 0$, $U_{22} = U_{11}$, and $U_{23} = U_{13} = 0$ for all atoms.
V [Å^3]: Volume of the coordination polyhedron [29].
CN (H): coordination number according to Hoppe [27, 29].
CN (O'K): coordination number according to O'Keeffe [28, 29].

Table 3: Interatomic bond distance (in Å) and average coordination distances for $Li_8Sb_xSn_{3-x}$. *X* is any atom in the coordination sphere of the central atom.

$Li_8Sb_xSn_{3-x}$					
*M*1–Li1	2.811(4), 2x	Li1–Li2	2.790(11)	Li3–Li4	2.839(10)
*M*1–Li4	2.870(3), 6x	Li1–*M*1	2.811(4)	Li3–Li1	2.861(3), 3x
*M*1–Li3	3.310(5), 6x	Li1–Li3	2.861(3), 3x	Li3–Li4	2.876(4), 3x
		Li1–*M*2	2.896(15), 3x	Li3–Li2	3.012(15)
*M*2–*M*2	2.8544(7)	Li1–Li4	3.294(6), 3x	Li3–*M*1	3.310(5), 3x
*M*2–Li4	2.889(8)	Li1–Li2	3.429(8), 3x	Li3–*M*2	3.328(5), 3x
*M*2–Li1	2.896(15), 3x				
*M*2–Li2	2.919(4), 3x	Li2–Li1	2.791(11)	Li4–Li3	2.839(10)
*M*2–Li2	3.240(6), 3x	Li2–Li2	2.798(5), 3x	Li4–*M*1	2.870(3), 3x
*M*2–Li3	3.328(5), 3x	Li2–*M*2	2.919(4), 3x	Li4–Li3	2.876(4), 3x
		Li2–Li3	3.012(15)	Li4–*M*2	2.889(8)
		Li2–*M*2	3.240(6), 3x	Li4–Li1	3.294(6), 3x
		Li2–Li1	3.429(8), 3x	Li4–Li4	3.300(9), 3x
first coordination sphere		second coordination sphere		total [14]-fold coordination	
$\langle M1^{[8]}–X\rangle$	2.855	$\langle M1^{[..+6]}–X\rangle$	3.311	$\langle M1^{[14]}–X\rangle$	3.051
$\langle M2^{[8]}–X\rangle$	2.899	$\langle M2^{[..+6]}–X\rangle$	3.284	$\langle M2^{[14]}–X\rangle$	3.064
$\langle Li1^{[8]}–X\rangle$	2.859	$\langle Li1^{[..+6]}–X\rangle$	3.362	$\langle Li1^{[14]}–X\rangle$	3.074
$\langle Li2^{[8]}–X\rangle$	2.869	$\langle Li2^{[..+6]}–X\rangle$	3.335	$\langle Li2^{[14]}–X\rangle$	3.069
$\langle Li3^{[8]}–X\rangle$	2.883	$\langle Li3^{[..+6]}–X\rangle$	3.319	$\langle Li3^{[14]}–X\rangle$	3.070
$\langle Li4^{[8]}–X\rangle$	2.871	$\langle Li4^{[..+6]}–X\rangle$	3.297	$\langle Li4^{[14]}–X\rangle$	3.053

a slightly lower R-value, but a partial substitution of Sb by Sn atoms lowering the Sb-content cannot be ruled out completely. A homogeneity range of $Li_8Sb_xSn_{3-x}$ up to approx. 9 at.% Sb which corresponds to full occupation of the *M1* site with Sb is compatible with our investigations of phase relations. Accordingly, the homogeneity range is given as $0.3 \leq x \leq 1.0$.

A further important aspect is the classification of $Li_8Sb_xSn_{3-x}$ either as a true ternary compound or as the solid solution of Sb in a hypothetic compound Li_8Sn_3 [8]. This question is coupled to the existence of the binary Li_8Sn_3 compound (cf. Section 1), which is suggested by the investigations of [8] and [9], who observed additional steps in the e.m.f. *vs.* composition curves at the relevant stoichiometry. However, data have been gained from coulometric titration which easily shows artificial potential steps caused by slow lithiation kinetics. Furthermore, no direct observation of this binary compound by XRD, thermal analysis or other methods is available so far. Accordingly, the most recent version of the phase diagram by Li et al. [7] does not include the binary Li_8Sn_3, as well as most of other phase diagrams hitherto published. Neither phase analysis of numerous samples in the binary system Li–Sn reported in Li et al. [7] nor our present investigations in the ternary system Li–Sb–Sn reveal any phase with a binary composition Li_8Sn_3.

Furthermore, our results indicate that $Li_8Sb_xSn_{3-x}$ qualifies as a ternary phase due to the existence of two- and three-phase fields between $Li_8Sb_xSn_{3-x}$, Li_3Sb and the neighboring Li–Sn compounds $Li_{13}Sn_5$ and Li_7Sn_2. In terms of thermal stability, the ternary compound was observed at 300 °C as well as at 400 °C.

3.3 The crystal structure of the title compound

The title compound crystallizes in the trigonal crystal system with space group $R\bar{3}m$ (no. 166) and the lattice parameters $a = 4.6962(11)$ and $c = 31.536(6)$ Å. It is structurally related to Li_8Pb_3 and $Li_6Cu_2Sn_3$ [11, 30]. The atomic arrangement within one unit cell is given in Figure 2.

Due to the fact that in $Li_8Sb_xSn_{3-x}$ only the sites 3(*a*) and 6(*c*) are occupied, all atoms within the unit cell are located on the (11 $\bar{2}$ 0) plane (Figure 3). The atoms within this plane form a regular arrangement: The crystal structure is composed by crystallographically identical but offset atom chains with rod symmetry $\mathcal{P}\bar{1}$ running parallel to [$\bar{1}\bar{1}$ 11 1] (one such chain is highlighted by a gray background in Figure 3). Each chain contains all atom types *M*1, *M*2, and Li1 to Li4, the repeating sequence consists of in total 11 atoms. The chains deviate only slightly from linearity; they are built by three building blocks formed by groups of atoms with distinct length and composition. With the simplification that the Li1 position is only occupied by

Li atoms, all the three building blocks start with a *M* atom (either Sb = *M*1 or Sn = *M*2 atom), followed by two or three Li atoms (designated 2s or 3s, respectively): 2s = *M*2–Li2–Li2, 3s = *M*2–Li1–Li3–Li4, and 3s′ = *M*1–Li4–Li3–Li1. Nevertheless, the Li1 position is distinguished from Li2 – Li4 in Tables and Figures.

The 2s and the 3s blocks start with a *M*2 atom followed by two and three Li atoms, respectively, while the 3s′ element is built from a *M*1 atom followed by three Li atoms arranged as the reverse of the Li sequence of 3s, because the *M*1 atom represents the inversion center of the rod group; i. e. the site symmetry $\bar{3}m$ of the compound's space group. Thereby, the whole crystal structure can be composed from these three different building blocks by forming the atom chains out of the sequence 3s, 3s′ and 2s that are in turn assembled into the layer by shifting (see Figure 3).

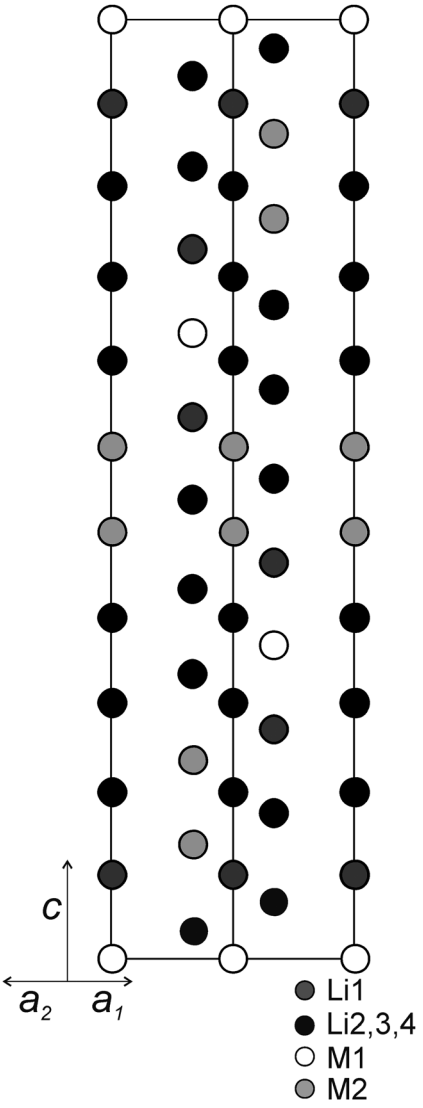

Figure 2: The crystal structure of $Li_8Sb_xSn_{3-x}$ in a projection along [$\bar{1}\bar{1}0$].

Further insight into the crystal structure is gained considering also the local environment of each atom in the chains, i. e. by extending the description to neighboring chains in the same layer as well as to those above and below. As a result, the crystal structure is described based on polyhedra sequences.

In $Li_8Sb_xSn_{3-x}$, the coordination number for each of the six different atoms is eight in the first coordination sphere (distorted cube) and six in the second one (distorted octahedron). The coordination figure may be described as a hexacapped cube [31] where the coordinating atoms represent the corners. This [8+6] coordination can be derived from the bcc W-structure type, which represents also the type structure of pure Li stable at ambient conditions (Figure 4 gives the coordination for each atom).

A transformation of the unit cell of trigonal $Li_8Sb_xSn_{3-x}$ according to [2/3 1/3 0.0602/–1/3 –2/3 0.0602/1/3 –1/3 –0.0602] results in the average cell with the metric a = 3.310, b = 3.310, c = 3.310 Å, α = 89.63, β = 89.63, γ = 90.37° which resembles cubic *pseudo*-symmetry; the unit is significantly smaller as compared to that given by Berliner et al. [32] for bcc-Li metal: a = 3.47851(1) Å. The cell volumes of the title compound and bcc-Li are 602.3 $Å^3$ (for 33 atoms per unit cell) and 42.09 $Å^3$ (Z = 2) giving 18.25 respectively 21.05 $Å^3$ per atom; it is worth noticing that the coordination polyhedra in bcc-Li are definitely larger.

Starting point for the following discussion is the hexacapped cube that only contains Li atoms. Note that in contrast to the ideal aristotype bcc-structure type the hexacapped cubes in the ternary compound does not exhibit a regular [14]-fold coordination (and consequently deviates from an Archimedean solid), but show a slight angular distortion besides some moderate differences in the bond lengths; moreover, the point symmetries of the coordination polyhedra are only $3m$ or $\bar{3}m$ in the title compound but $m\bar{3}m$ in Li metal.

Various hexacapped cubes centered by Li atoms but coordinated by various arrangements of Li, Sn (or Pb) atoms, respectively, were discussed and classified by Frank and Müller [33] who assigned the letters "a" to "n" to the various resulting hexacapped cubes. These authors focused on Li-centered hexacapped cubes occurring in Li-plumbides and –stannides, but a systematic classification for Sn- or Pb-centered hexacapped cubes is still missing. Furthermore, they studied the occurrence of various hexacapped cubes in the crystal structures of Li-plumbides and –stannides, but did not analyze the structures for any repeating hexacapped cube sequences.

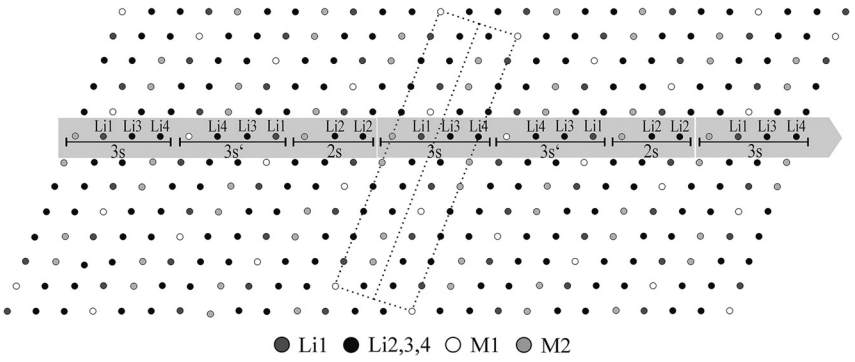

Figure 3: The (1 1 $\bar{2}$ 0) plane in the crystal structure of $Li_8Sb_xSn_{3-x}$, parallel to the direction [$\bar{1}$1 1 1]. The 3s3s′2s atomic sequence is highlighted by a gray background. Combining this sequence to chains respectively to planes, the entire crystal structure is formed. The unit cell is indicated by dotted lines (analogue projection as in Figure 2).

$Li_8Sb_xSn_{3-x}$ exhibits two hexacapped cubes S1 and S2 centered by *M*1 and *M*2 atoms, respectively (Tables 4 and 5); the hexacapped cube centered by an *M*1 atom is only coordinated by Li atoms, while the one centered by an *M*2 atom contains another *M*2 atom in the first coordination sphere (see Figure 4).

The atom sequences along [$\bar{1}$1 11 1] discussed above can be extended to the respective hexacapped cubes sequence; the nomenclature applied by Frank and Müller [33] for the coordination polyhedra of the $Li^{[8+6]}$ atoms is given in analogy for the *M*-centered hexacapped cubes designed as S1 (coordinated by Li atoms only) and S2 (coordinated by an *M*2 atom in the first coordiantion sphere besides Li atoms), respectively (see Tables 4, 5, Figure 5). Like the building blocks defined for the atom sequences, each hexacapped cube sequence starting with S1 or S2 defines the corresponding hexacapped cube building block (Figure 5). For clarity, only every second polyhedron is expressed by sticks. The hexacapped cube sequence is constructed similar to the 3s3s′2s atom sequence, (Figure 5). Thereby, the hexacapped cubes are ordered along the 3s3s′2s-sequence using the *M* and Li atoms as central atoms that are coordinated by the hexacapped cube types according to the scheme from Frank and Müller [33] as listed in Table 4.

The 3s3s′2s atom sequence and the corresponding hexacapped cube sequence reflect the composition of the title compound Li:Sb:Sn = 8:1:2 (neglecting minor

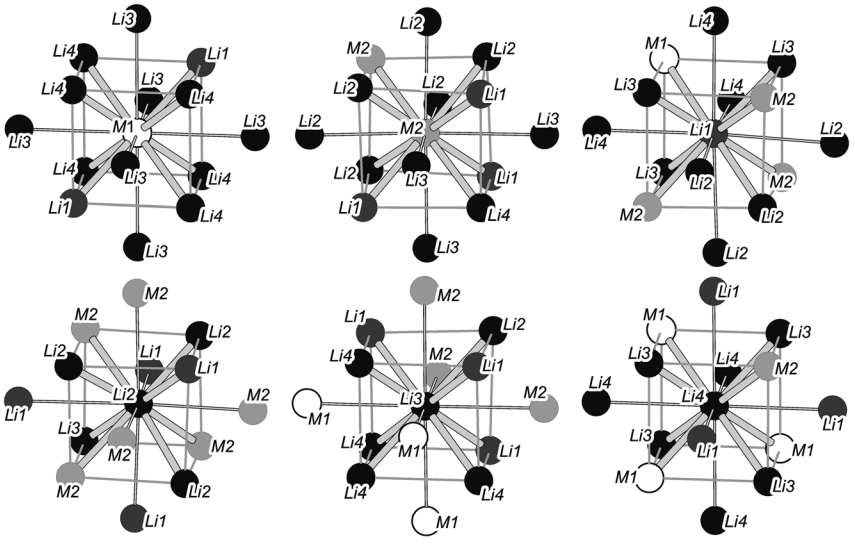

Figure 4: Polyhedral environment for all atoms in the crystal structure of the ternary compound $Li_8Sb_xSn_{3-x}$. The observed Li centered coordination polyhedra correspond with that described by [31] (see Table 4 and text). The atoms *M1* and *M2* were added as the title compound can be derived from the W-type structure as characteristic for Li under ambient conditions.

Table 4: Central atom, number of ligands and nomenclature for the various polyhedra in $Li_8Sb_xSn_{3-x}$.

Central Atom	Ligands	Nomenclature according to [33]
Li1	[10 Li + 1 *M*1 + 3 *M2*]	b
Li2	[4 Li + 4 Li1 + 6 *M*2]	d
Li3	[5 Li + 3 Li1 + 3*M*1 + 3 *M*2]	a
Li4	[7 Li + 3 Li1 + 3 *M*1 + 1 *M*2]	b
		Nomenclature from this work
*M*1	[13 Li + 1 Li1]	S1
*M*2	[10 Li + 3 Li1 + 1 *M*2]	S2

Table 5: Correlation between atom sequence and polyhedra sequence.

Designation	Atom sequence	Polyhedra sequence
3s	*M*2–Li1–Li3–Li4	S2-b-a-b
3s′	*M*1–Li4–Li3–Li1	S1-b-a-b
2s	*M*2–Li2–Li2	S2-d-d

atom substitutions and/or mixed positions and tentative vacancies). Due to the fact that the compositions of Li–Sn phases neighbored in the phase diagram differ by a few at % only, similar atom environments as well as analogue atomic and hexacapped cube sequences are likely.

For a topological comparison, not only the occurrence of analogue hexacapped cubes but also of comparable 1D-atomic and 1D-hexacapped cube sequences, respectively, is considered. Each sequence is defined starting with the *M*-centered hexacapped cube (*M* is either a Sn- or Sb atom), followed by only Li-centered hexacapped cubes (not taking into account any mixed occupancies).

Applying these principles to the atomic arrangement in $Li_{13}Sn_5$ [33] and Li_5Sn_2 [34] revealed that both crystal structures can be described by analogue S1/S2–b–a–b and S2–d–d sequences only (Table 6) whereby both atomic positions, *M1* and *M2* are occupied by Sn only. However, the ratio of the individual building blocks differs to achieve the respective Sn:Li ratios. The structural and topological relationship to the other Li-Sn phases known so far in the Li-rich as well as in the Sn-rich area, requires extended discussion; it will be conducted elsewhere.

Within this group formed by the three compounds it can be observed that $M1^{[8+6]}$ atoms are coordinated by Li atoms only (labeled S1) but $M2^{[8+6]}$ atoms have one *M* atom besides Li atoms within their first coordination sphere (labeled S2). In the crystal structure of cubic Li_3Sb [14] only the sequence S1-b-a-b occurs, i. e. the 3s′ block with Sb at the *M1* position forms the entire atomic arrangement (see Table 6). This is consistent with the ternary title compound $Li_8Sb_xSn_{3-x}$: the site multiplicity of the *M*1 and *M*2 position and the structure refinements suggest an allocation of the *M*1 and *M*2 positions predominantly by Sb and Sn atoms, respectively. The occurrence of S1 in $Li_{13}Sn_5$ shows that this cuboctahedron can also be centered by Sn, which may suggest a mixed occupancy by Sb and Sn in S1 in $Li_8Sb_xSn_{3-x}$, which explains the difference between the ordered stoichiometry "Li_8SbSn_2" (~9 at.% Sb) from SC-XRD and the ~3–4 at.% Sb

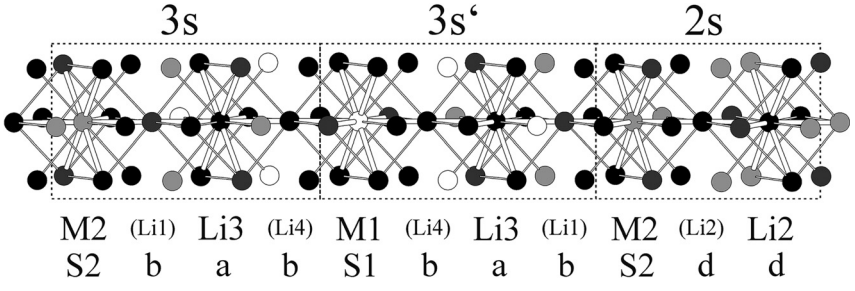

Figure 5: The hexacapped cubes around atoms along [$\overline{1}$1 1] in $Li_8Sb_xSn_{3-x}$. For clarity, the hexacapped cube of only every second central atom is drawn. The sequences of central atoms and hexacapped cubes are indicated.

Table 6: Polyhedra sequence in the title compound and phases with similar ratios *M*:Li.

Compounds	Polyhedra sequence/atom sequence				
$Li_8Sb_xSn_{3-x}$ [this work]	S2-b-a-b/3s	S1-b-a-b/3s′	S2-d-d/2s		
$Li_{13}Sn_5$ [31]	S2-b-a-b/3s	S1-b-a-b/3s′	S2-d-d/2s	S2-b-a-b/3s	S2-d-d/2s
Li_5Sn_2 [32]	S2-b-a-b/3s	S2-d-d/2s			
c-Li_3Sb [12, 13]	S1-b-a-b/3s′				

according to our preliminary phase diagram analysis. In any case, Sb only centers the S1 hexacapped cube.

Recently the crystal structure of $Li_6Cu_2Sn_3$ was published by Fürtauer et al. [30]. Despite the different stoichiometry and the presents of copper, its crystal structure is isotypic to $Li_8Sb_xSn_{3-x}$; however, the atom distribution over the various atom sides differs: the two M-position of $Li_8Sb_xSn_{3-x}$ are occupied by Sn in $Li_6Cu_2Sn_3$; Li3 corresponds to Li1* (the "*" denotes positions from $Li_6Cu_2Sn_3$), which are only occupied by lithium in both structures, the remaining Li-positions have mixed Li + Cu occupancies in $Li_6Cu_2Sn_3$.

Fürtauer and co-works [30] characterized this structure by different layers composed of face-sharing octahedra, tetrahedra and trigonal prisms. $Li_6Cu_2Sn_3$ can be described by the repeated sequence of three layers: A_1-B-A_1, where A_1 is made from ocathedra and tetrahedra, while B contains trigonal prisms. While at first glance this description differs from ours, the similarity can be established through identification of A_1-B-A_1 with our atom sequence 3s2s 3s′ = 3s3s′ 2s. In complete analogy the layer sequences A_1-B-A_1-B-A_1 given for $Li_{13}Sn_5$ and A_1-B for Li_5Sn_2 in [30] correspond to 3s3s′2s3s2s and 3s2s.

4 Conclusion

It is expected that atomic environments in adjacent compounds in phase diagrams may be comparable and consequently, their crystal structures exhibit similarities to some extent. As shown in this work, the title compound is derivable from the bcc structure type of the common Li modification: parts of the Li atoms are substituted by Sb or Sn atoms, the cubic cell is trigonal rhombohedrally distorted and the unit-cell volume is increased. It is demonstrated that the crystal structures of ternary compounds may be described by building blocks related to these observed in the binary constituent phase diagrams.

The compounds $Li_{13}Sn_5$, Li_5Sn_2 and $Li_8Sb_xSn_{3-x}$ are built from the hexacapped cube-types a, b, d, S1 and S2. However, the crystal structures of these compounds are characterized by distinct sequences of the larger building blocks designated 3s, 3s′ and 2s. The cubic modification of Li_3Sb exhibits an S1-b-a-b sequence that builds up the entire crystal structure. Additionally, as this building block is identical to that in the ternary compound, we assume that Sb atoms predominantly occupy the *M*1 position in $Li_8Sb_xSn_{3-x}$. The admixture of Sn at this position cannot be ruled out since S1 building blocks with Sn at the *M1* position occur in $Li_{13}Sn_5$. Thus, these crystal structures exhibit rather general similarities with respect to their topology.

The structure models involving the hexacapped cubes labelled a, b, d, S1 and S2, as well as the building blocks 3s, 3s′ and 2s, respectively, is applicable to the compounds mentioned above. However, the topological description of Li-rich as well as Sn-rich alloys requires additional polyhedra types [33]. A further investigation of the structural relations between the ternary compound $Li_8Sb_xSn_{3-x}$ and the binary Li–Sn phases is currently in progress.

Acknowledgment: We thank Mr. P. Wibner for doing preliminary experiments.

Author contribution: All the authors have accepted responsibility for the entire content of this submitted manuscript and approved submission.

Research funding: This work was supported by the DFG project FL-730/1-2 within the priority program SPP 1473, "WeNDeLIB".

Conflict of interest statement: The authors declare no conflicts of interest regarding this article.

References

1. Zhang W. J. A review of the electrochemical performance of alloy anodes for lithium-ion batteries. *J. Power Sources* 2011, *196*, 13.
2. Winter M., Besenhard J. O. Electrochemical lithiation of tin and tin-based intermetallics and composites. *Electrochim. Acta* 1999, *45*, 31.
3. Wachtler M., Besenhard J. O., Winter M. Tin and tin-based intermetallics as new anode materials for lithium-ion cells. *J. Power Sources* 2001, *94*, 189.
4. Trifonova A., Wachtler M., Winter M., Besenhard J.O. Sn-Sb and Sn-Bi alloys as anode materials for lithium-ion batteries. *Ionics* 2002, *8*, 321.
5. Sougrati M. T., Fullenwarth J., Debenedetti A., Fraisse B., Jumas J. C., Monconduit L. TiSnSb a new efficient negative electrode for Li-ion batteries: mechanism investigations by operando-XRD and Mössbauer techniques. *J. Mater. Chem.* 2011, *21*, 10069.
6. Marino C., Sougrati M. T., Darwiche A., Fullenwarth J., Fraisse B., Jumas J. C., Monconduit L. Study of the series $Ti_{1-y}Nb_ySnSb$ with $0 \leq y \leq 1$ as anode material for Li-ion batteries. *J. Power Sources* 2013, *244*, 736.
7. Li D., Fürtauer S., Flandorfer H., Cupid D.M. Thermodynamic assessment and experimental investigation of the Li-Sn system. *Calphad* 2014, *47*, 181.
8. Gasior W., Moser Z., Zakulski W. Thermodynamic studies and the phase diagram of the Li-Sn system. *J. Non-Cryst. Solids* 1996, *205*, 379.
9. Giel H., Henriques D., Markus T. Investigations of the Li_8Sn_3 phase in the binary Li-Sn system using an improved coulometric-titration setup. *J. Electrochem. Soc.* 2017, *164*, A907.
10. Zalkin A., Ramsey W., Templeton D. Intermetallic compounds between lithium and lead. II. The crystal structure of Li_8Pb_3. *J. Chem. Phys.* 1956, *60*, 1275.

11. Cenzual K., Gelato L. M., Penzo M., Parthé E. Overlooked trigonal symmetry in structures reported with monoclinic centred Bravais lattices; trigonal description of Li_8Pb_3, PtTe, Pt_3Te_4, Pt_2Te_3, $LiFe_6Ge_4$, $LiFe_6Ge_5$, $CaGa_6Te_{10}$ and $La_{3.266}Mn_{1.1}S_6$. *Z. Kristallogr.* 1990, *193*, 217.
12. Mayo M., Morris A. J. Structure prediction of Li-Sn and Li-Sb intermetallics for lithium-ion batteries anodes. *Chem. Mater.* 2017, *29*, 5787.
13. Beutl A., Cupid D., Flandorfer H. The Li-Sb phase diagram part I: new experimental results. *J. Alloys Compd.* 2017, *695*, 1052.
14. Brauer G., Zintl E. Konstitution von Phosphiden, Arseniden, Antimoniden und Wismutiden des Lithiums, Natriums und Kaliums. *Z. Phys. Chem.* 1937, *37*, 323.
15. Saubanere M., Ben Yahia M., Lemoigno F., Doublet M. L. Influence of polymorphism on the electrochemical behavior of M_xSb negative electrodes in Li/Na batteries. *J. Power Sources* 2015, *280*, 695.
16. Schmetterer C., Polt J., Flandorfer H. The phase equilibria in the Sb-Sn system - Part I: literature review. *J. Alloys Compd.* 2017, *728*, 497.
17. Schmetterer C., Polt J., Flandorfer H. The phase equilibria in the Sb-Sn system - Part II: experimental results. *J. Alloys Compd.* 2018, *743*, 523.
18. Rönnebro E., Yin J., Kitano A., Wada M., Sakai T. Comparative studies of mechanical and electrochemical lithiation of intermetallic nanocomposite alloys for anode materials in Li-ion batteries. *Solid State Ionics* 2005, *176*, 2749.
19. Rönnebro E., Yin J., Kitano A., Wada M., Tanase S., Sakai T. Reaction mechanism of a $Ag_{36.4}Sb_{15.6}Sn_{48}$ nanocomposite electrode for advanced Li-ion batteries. *J. Electrochem. Soc.* 2005, *152*, A152.
20. Wilson A. J. C. *International Tables for X-ray Crystallography*; Kluver: Dordrecht, The Netherlands, 1992.
21. Otwinowski Z., Minor W. Processing of X-ray diffraction data collected in oscillation mode. *Method. Enzymol.* 1997, *276*, 307.
22. Hooft R. W. W. *Collect*; Nonius BV: Delft, The Netherlands, 1999.
23. Sheldrick G. M. *SHELXS-97, A Program for the Solution of Crystal Structures*; University of Göttingen: Germany, 1997.
24. Sheldrick G. M., *SHELXL-97, A Program for Crystal Structure Refinement*; University of Göttingen: Germany, 1997.
25. Sheldrick G. M. A short history of SHELX. *Acta Crystallogr. A* 2008, *64*, 112.
26. Sheldrick G. M. SHELXT – Integrated space group and crystal-structure determination. *Acta Crystallogr. A* 2015, *71*, 3.
27. Hoppe R. Die Koordinationszahl – ein "anorganisches Chamäleon". *Angew. Chem.* 1970, *82*, 7.
28. O'Keeffe M. A proposed rigorous definition of coordination number. *Acta Crystallogr. A* 1979, *35*, 772.
29. Nowotny H., Zobetz E. "*Kristallchemie". Program for Solving Geometrical Problems in Crystal Structures*; University of Vienna: Austria, 1982.
30. Fürtauer S., Effenberger H.S., Flandorfer H. New intermetallic phases in the Cu–Li–Sn system: the lithium-rich phases Li_3CuSn and $Li_6Cu_2Sn_3$. *Z. Kristallogr.* 2016, *231*, 79.
31. FIZ Karlsruhe A Focus on Crystallography; FIZ Karlsruhe: Germany, 2015. https://www.fiz-karlsruhe.de/sites/default/files/FIZ/Dokumente/Broschueren/A-Focus-on-Crystallography.pdf (accessed Jan 29, 2020).
32. Berliner R., Fajen O., Smith H. G., Hitterman R. L. Neutron powder-diffraction studies of lithium, sodium and potassium metal. *Phys. Rev. B* 1989, *40*, 12086.
33. Frank U., Müller W. Darstellung und Struktur der Phase $Li_{13}Sn_5$ und die strukturelle Verwandtschaft der Phasen in den Systemen Li-Sn und Li-Pb. *Z. Naturforsch.* 1975, *30b*, 316.
34. Frank U., Müller W., Schäfer H. Die Struktur der Phase Li_5Sn_2. *Z. Naturforsch.* 1975, *30b*, 1.